

Recalculation of Pion Compton Scattering in Perturbative QCD

Ding-fang Zeng

Department of Physics, Peking University, Beijing 100871, China

Bo-Qiang Ma

CCAST (World Laboratory), P.O. Box 8730, Beijing 100080, China,

and Department of Physics, Peking University, Beijing 100871, China^{*}

December 8, 2018

Abstract

We recalculated pion virtual Compton scattering in perturbative QCD in this paper. Our calculation clarified some doubtful points in existing literatures, and treated real Compton scattering as a limit case in which the mass of the virtual photon equals to zero. By comparing the effects of different distribution amplitudes on the prediction of physical observables, we indicate that behavior of the distribution amplitudes in the very end point region does not have very important effects on the physical prediction.

1 Introduction

Pion virtual Compton scattering (VCS) $\gamma^*\pi^- \rightarrow \gamma\pi^-$ via the reaction $e\pi^- \rightarrow e\gamma\pi^-$ is observed by SELEX Collaboration at Fermi Lab [1] for the first time. Although in the current available kinematical region, the process can not be predicted precisely in perturbative QCD (pQCD), it is possible to observe such processes in the pQCD-applicable region with the quick development of experimental techniques. Therefore it is meaningful to check the pQCD prediction of this process.

^{*}Mailing address.

For this problem, Tamazouzt [2] calculated a very similar process, $\gamma\pi^\pm \rightarrow \gamma^*\pi^\pm$; Maina and Torrasso [3] calculated it directly and treated the singular integration appearing in it carefully; Li and Coriano [7] calculated it by a rather different way. One common problem existing in [2] and [7] is: the authors only directly calculated 5 diagrams contributing to the unintegrated amplitude but gave no prescriptions about how to get the other 15 ones, please see fig.2 and captions there. Ref.[3] did not give its expressions for the unintegrated amplitude but claimed consistence with [2].

From the results that, the two polarized cross sections $\frac{d\sigma_{RR}}{d\cos\theta}$ and $\frac{d\sigma_{LR}}{d\cos\theta}$ of real Compton scattering (RCS) have almost the same scattering angle dependence, we doubt that the author of [2] got the other 15 diagrams contributing to H correctly, please see fig.2 of [2]. As we will indicate in the following, the number of independent diagrams is 10, instead of 5 in this problem, please see fig.2. Of course the total number is 20. As was pointed out by [3], the numerical treatment of [2] has some defaults. However, the revised results still have some doubtful points. First, the cross section $S^3 \frac{d\sigma_{+R}}{d\cos\theta} |_{v \rightarrow 0} \rightarrow 0$, as we will indicate in this paper, this is not the case. Second, the nearly jumping change appearing in the phase of M_{LR} , please see fig.5 of [3]. Third, transferring from VCS to RCS is the very unnatural, please see fig.1 of [3].

Because of these questions in the literatures, we decide to recalculate this problem in this paper. It will be shown that such doubtful aspects do not exist in our recalculated results.

2 Factorization Theorem of pQCD for Pion VCS

As indicated in the caption of fig.1, a complete physical process $e\pi^- \rightarrow e\gamma\pi^-$ can take place through two ways, Bethe-Heitler process and virtual Compton scattering. But we will not calculate such a complete process in this paper, please refer to [3] and [4]. We will concentrate on the sub-process $\gamma^*\pi^\pm \rightarrow \gamma\pi^\pm$ and use M to denote the amplitude of it. Besides its inclusion of real Compton scattering as a limit case, it is also meaningful in the preparation for the calculation of the complete process $e\pi^- \rightarrow e\gamma\pi^-$.

Factorization theorem states that for an exclusive process [8] such as pion VCS

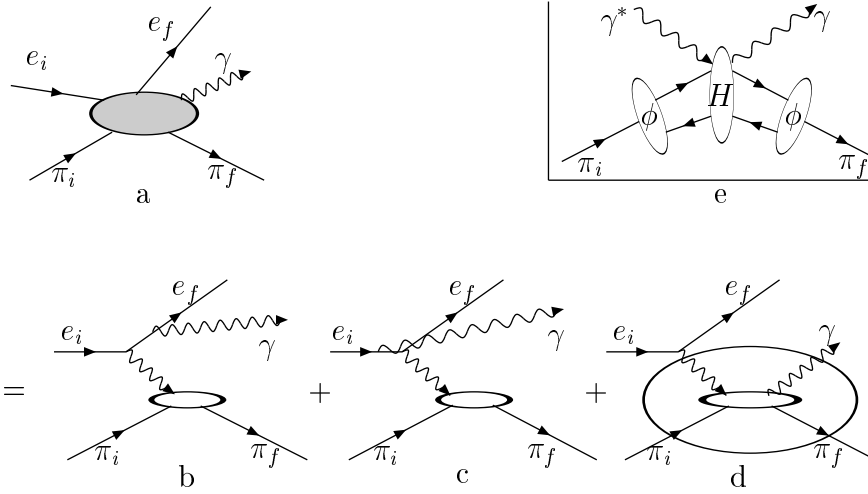


Figure 1: Reaction (a) $e\pi^\pm \rightarrow e\gamma\pi^\pm$ can proceed both through (b)&(c) Bethe-Heitler process and through (d) virtual Compton scattering. In experiments, the two kinds of process can not be separately detected. When the pion momentum change is large enough in the process (d) $\gamma^*\pi^\pm \rightarrow \gamma\pi^\pm$ can be factorized as (e) $M = \int dx dy \phi(x) H(x, y) \phi(y)$, where H can be computed perturbatively, please see fig.2.

$\gamma^*\pi^\pm \rightarrow \gamma\pi^\pm$, the amplitude of it can be written as the following convolution formula,

$$M(p; \epsilon q \rightarrow p'; \epsilon' q') = \int dx dy \phi(x, Q) H(xp; \epsilon, q \rightarrow yp'; \epsilon', q') \phi(y, Q), \quad (1)$$

where p denotes the momentum of the incoming pion, ϵ and q are the polarization vector and momentum of the photon respectively. x denotes one of the momentum fraction of the valence quarks in the incoming pion, and that of the other one will be denoted by $\bar{x} = 1 - x$. The primed variables or y are associated with outgoing particles.

The pion distribution amplitude $\phi(x, Q)$ in eq.(1) absorbs the long-distance dynamics of M and can be derived by non-perturbative methods [10]. Appearing of Q in it indicates its evolution with the energy scale. In this paper, instead of consideration of such evolution [7, 9], we will study the following five phenomenological models and their effects on the physics predictions [11, 12, 13, 15],

$$\begin{aligned} \phi_{as} &= f_\pi x(1-x), \\ \phi_{bhl} &= 1.8067 f_\pi x(1-x) \exp\left[-\frac{0.07043}{x(1-x)}\right], \\ \phi_{cz} &= 5 f_\pi x(1-x)(2x-1)^2, \end{aligned}$$

$$\begin{aligned}
\phi_{hs} &= 10.7246 f_\pi x(1-x)(2x-1)^2 \exp\left[-\frac{0.07062}{x(1-x)}\right], \\
\phi_{p3} &= f_\pi x(1-x)[0.6016 - 4.659(2x-1)^2 + 15.52(2x-1)^4],
\end{aligned} \tag{2}$$

with the pion decay constant $f_\pi = 133$ MeV, please see fig.4 for their explicit shapes. From the figure, we can see that, relative to ϕ_{as} and ϕ_{cz} , the distribution amplitudes ϕ_{bhl} and ϕ_{hs} suppress the end point region deeply, while function ϕ_{p3} intensifies both the near-end-point region and the center region.

Contrary to $\phi(x)$, the hard amplitude $H(xp; \epsilon q \rightarrow yp'; \epsilon' q')$ in eq.(1) absorbs short-distance dynamics of the amplitude, and can be calculated perturbatively on the basis of the diagrams in fig.2. With leading Fock state of π^+ (π^- case is similar),

$$|\pi^+(p)\rangle = \frac{1}{\sqrt{2}} \frac{1}{\sqrt{3}} \sum_i^{1,2,3} \left(|u_\uparrow^i(xp)\rangle |\bar{d}_\downarrow^i(\bar{x}p)\rangle + |u_\downarrow^i(xp)\rangle |\bar{d}_\uparrow^i(\bar{x}p)\rangle \right), \tag{3}$$

where i and \bar{i} denote the color indices, H can be written as

$$\begin{aligned}
H(xp, \epsilon q \rightarrow yp', \epsilon' q') &\sim \\
&\sum_{diag. color} \sum \frac{1}{2} \frac{1}{3} \left[\frac{\bar{u}_\uparrow^j(yp') (\dots \gamma^\mu t_{ji}^a \dots) u_\uparrow^i(xp) g_{\mu\nu} \delta^{ab} \bar{v}_\downarrow^{\bar{i}}(\bar{x}p) (\dots \gamma^\nu t_{\bar{i}\bar{j}}^b \dots) v_\downarrow^{\bar{j}}(\bar{y}p')}{p_1^2 p_2^2 p_3^2} \right. \\
&\quad \left. + \frac{\bar{u}_\downarrow^j(yp') (\dots \gamma^\mu t_{ji}^a \dots) u_\downarrow^i(xp) g_{\mu\nu} \delta^{ab} \bar{v}_\uparrow^{\bar{i}}(\bar{x}p) (\dots \gamma^\nu t_{\bar{i}\bar{j}}^b \dots) v_\uparrow^{\bar{j}}(\bar{y}p')}{p_1^2 p_2^2 p_3^2} \right], \tag{4}
\end{aligned}$$

with the coupling constants α_e , α_s and the charge factor e_u^2 or $e_u e_d$ suppressed for the moment. In eq.(4), p_1 , p_2 and p_3 denote the momentum transferred through the two fermion and one gluon propagators; explicit expressions of $(\dots \gamma^\mu t^a \dots)$ s depend on the details of diagrams. Using identity of $SU(3)$ color group,

$$t_{ij}^a t_{kl}^a = \frac{1}{2} (\delta_{il} \delta_{jk} - \frac{1}{3} \delta_{ij} \delta_{kl}), \tag{5}$$

and some trace making trick, please see [17], eq.(4) can be transformed into the following form

$$\begin{aligned}
H(x, \epsilon q \rightarrow y, \epsilon' q') &= \sum_{diag.} H_{\epsilon\epsilon'}^{(diag.)} \\
&= \frac{2}{3} \sqrt{x\bar{x}y\bar{y}} \sum_{diag.} Tr[(\gamma^\mu \dots)_{diag.} \gamma^5 \not{p} (\gamma_\mu \dots)_{diag.} \gamma^5 \not{p'}]. \tag{6}
\end{aligned}$$

By the usual convention, distribution amplitude $\phi(x)\phi(y)$ will absorb the $\sqrt{x\bar{x}y\bar{y}}$ factor, so it will not be included in our later expressions for $H_{\epsilon\epsilon'}$.

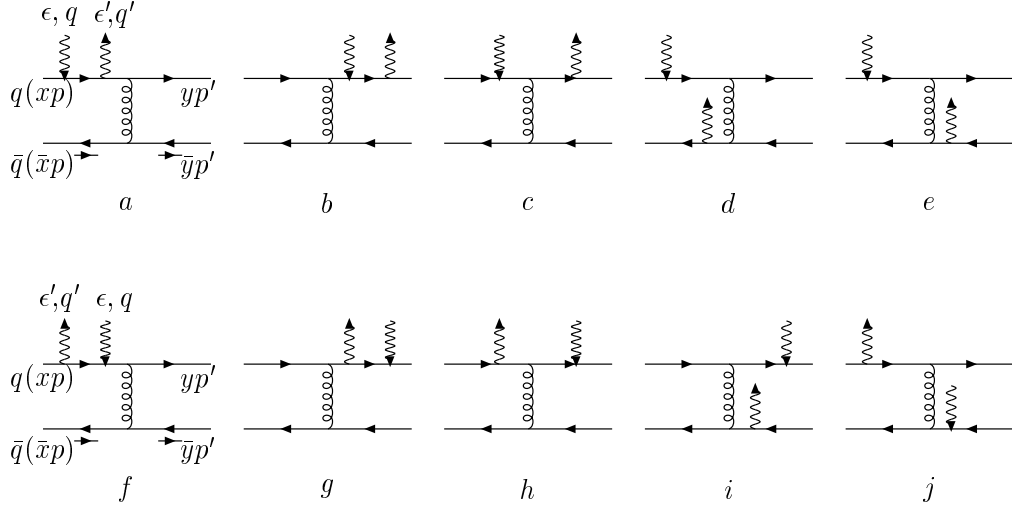


Figure 2: Unintegrated (hard) amplitude H can be calculated on the basis of these diagrams. Complete H includes other ten diagrams with the photons attaching to different quark lines, and contributions of those diagrams to the full amplitude M are equal to the above ones except some charge factors.

3 Unintegrated Amplitude of $\gamma^* \pi^\pm \rightarrow \gamma \pi^\pm$

In the center-of-momentum frame of outgoing particles γ and π^\pm , please refer to [4], we write all the relevant kinematical variables as follows,

$$\begin{aligned}
 p'^\mu &= \frac{\omega + p}{2}(1, -\sin \theta, 0, -\cos \theta), \\
 q'^\mu &= \frac{\omega + p}{2}(1, \sin \theta, 0, \cos \theta); \\
 p^\mu &= (p, 0, 0, -p), q^\mu = (\omega, 0, 0, p); \\
 \epsilon_R^\mu &= \frac{1}{\sqrt{2}}(0, -1, -i, 0), \epsilon_R'^\mu = \frac{1}{\sqrt{2}}(0, -\cos \theta, -i, \sin \theta); \\
 \epsilon_L^\mu &= \frac{1}{\sqrt{2}}(0, 1, -i, 0),
 \end{aligned} \tag{7}$$

$$\epsilon_0^\mu = \frac{1}{\sqrt{2}}(1, 0, 0, 0). \tag{8}$$

Obviously, θ denotes the scattering angle of the process. According to parity invariance and gauge invariance, we only need to calculate three helicity amplitudes for the purpose of computing the amplitude of the complete physical process $e\pi^\pm \rightarrow$

$e\gamma\pi^\pm$, please see [3] and [4]. In order to compare with [2], we choose to calculate H_{RR} , H_{LR} and H_{0R} , while obtain the other three by the following relations,

$$H_{LL} = H_{RR}, \quad H_{RL} = H_{LR}, \quad H_{-L} = H_{+R}, \quad H_{-R} = -vH_{+R}. \quad (9)$$

After introducing the abbreviation $c = \cos \frac{\theta}{2}$, $s = \sin \frac{\theta}{2}$, $S = (\omega + p)^2$, $v = q^\mu q_\mu / S$ and $\bar{v} = 1 - v$, we can write all the diagrams contributing to H in more economical forms. The results are shown in table 1-3, where we have transformed the diagrams with two propagators potentially on shell into some equivalent forms in which only one of them can go on shell by the following relation,

$$\frac{f(x, y)}{(x - a(y) + i\epsilon)(x - b(y) + i\epsilon)} = \frac{f(x, y)}{a(y) - b(y)} \left(\frac{1}{x - a(y) + i\epsilon} - \frac{1}{x - b(y) + i\epsilon} \right). \quad (10)$$

This is very important in the numerical integration.

Table 1 $H_{RR}^{(diag.)}(\frac{1}{S}\alpha_e\alpha_s)$

$a :$	$\frac{4c^2s^{-2}\bar{v}^{-1}}{x\bar{y}(x-a-i\epsilon)}$	$f :$	$\frac{4s^{-2}\bar{v}^{-1}}{x\bar{x}\bar{y}}$
$b :$	$\frac{4c^2s^{-2}\bar{v}^{-1}}{\bar{x}\bar{y}\bar{y}}$	$g :$	$\frac{4c^2s^{-2}\bar{v}^{-1}}{\bar{x}\bar{y}[(1-\bar{v}s^2)y-v]}$
$c :$	$\frac{-4c^2s^{-2}\bar{v}^{-1}}{\bar{x}\bar{y}\bar{y}(x-a+i\epsilon)}$	$h :$	$\frac{-4s^{-2}\bar{v}^{-1}[1-(\bar{v}x+y)s^2+2\bar{v}xys^4]}{[y(1-\bar{v}s^2)-v]x\bar{x}\bar{y}}$
$d :$	$\frac{4\bar{v}^{-1}[c^2+s^2(\bar{v}x+v)]}{\bar{x}y} \left(\frac{1}{x-a+i\epsilon} - \frac{1}{x-b+i\epsilon} \right)$	$i :$	$\frac{-4c^2}{\bar{y}[y(1-\bar{v}s^2)-v](x-b+i\epsilon)}$
$e :$	0	$j :$	$\frac{4s^2\bar{v}^{-1}[y-\bar{v}(1+x-2x(1-y)s^2)]}{\bar{x}(1-ys^2)[y(1-\bar{v}s^2)-v](x-b+i\epsilon)}$
$a = -\frac{v}{\bar{v}}, b = \frac{y-v-ys^2}{\bar{v}(1-ys^2)}$			

Table 2 $H_{LR}^{(diag.)}(\frac{1}{S}\alpha_e\alpha_s)$

$a :$	$\frac{4\bar{v}^{-1}}{\bar{x}\bar{y}(x-a+i\epsilon)}$	$f :$	0
$b :$	$\frac{4\bar{v}^{-1}}{\bar{x}\bar{y}\bar{y}}$	$g :$	$\frac{4v\bar{v}^{-1}}{\bar{x}\bar{y}[(1-\bar{v}s^2)y-v]}$
$c :$	0	$h :$	$\frac{-4[y+\bar{v}x(1-2ys^2)]}{x\bar{x}\bar{y}[(1-\bar{v}s^2)y-v]}$
$d :$	$\frac{4s^2}{y} \left(\frac{1}{x-a+i\epsilon} - \frac{1}{x-b+i\epsilon} \right)$	$i :$	$\frac{-4c^2s^2y}{\bar{y}(1-ys^2)[(1-\bar{v}s^2)y-v](x-b+i\epsilon)}$
$e :$	$\frac{-4s^2c^{-2}\bar{v}}{y\bar{y}} \left(\frac{1}{x-a+i\epsilon} - \frac{1}{x-b+i\epsilon} \right)$	$j :$	$\frac{-4\bar{v}^{-1}s^2[y-\bar{v}x(1-2ys^2)]}{\bar{x}(1-ys^2)[(1-\bar{v}s^2)y-v](x-b+i\epsilon)}$

Table 3 $H_{+R}^{(diag.)}(\frac{1}{S}\alpha_e\alpha_s)$

$a :$	$\frac{8cs^{-1}}{\bar{x}\bar{y}}$	$f :$	$\frac{4cs^{-1}v\bar{v}^{-1}}{\bar{x}\bar{y}[(1-\bar{v}s^2)y-v]}$
$b :$	$\frac{cs^{-1}\bar{v}^{-1}}{\bar{x}\bar{y}\bar{y}}$	$g :$	$\frac{4c^{-1}s^{-1}\bar{v}^{-1}(1-2\bar{v}x)}{x}\bar{x}\bar{y}$
$c :$	$\frac{-4cs^{-1}}{\bar{x}\bar{y}\bar{y}}$	$h :$	$\frac{-4cs^{-1}\bar{v}^{-1}y(1-2\bar{v}s^2x)}{x\bar{x}[y(1-\bar{v}s^2)-v]}$
$d :$	$\frac{-4c^{-1}sv^{-1}[1-2\bar{v}s^2\bar{x}]}{\bar{x}(1-ys^2)(x-b+i\epsilon)}$	$i :$	$\frac{-4c^3sy}{\bar{y}(1-ys^2)[y(1-\bar{v}s^2)-v](x-b+i\epsilon)}$
$e :$	$\frac{4cs}{\bar{y}(1-2ys^2)(x-b+i\epsilon)}$	$j :$	$\frac{-4cs\bar{v}^{-1}[v(1-2s^2x\bar{y})-\bar{y}(1-2s^2x)]}{\bar{x}(1-ys^2)[y(1-\bar{v}s^2)-v](x-b+i\epsilon)}$

For $H_{RR}^{(diag.)}$ and $H_{LR}^{(diag.)}$, we compared our expressions with those of [2] in the $v \rightarrow 0$ limit (in [2], it is $R_b \rightarrow 0$). Except our consideration of 5 additional independent diagrams labelled $f \rightarrow j$, all the other terms, labelled $a \rightarrow e$, coincide with [2]. Note the singular points appearing in H_{LR} , the numerical results will indicate that in the integration, imaginary parts originating from them will cancel each other, in the $v \rightarrow 0$ limit, please see fig.5. Some relevant argument concerning this point can be found in the literature [18].

For $H_{0R}^{(diag.)}$, because we employ the convention of [3] for the virtual photon polarization vector, which is different from [2], our expressions of it does not coincide with that of [2]. Our convention is very convenient for future calculation of the complete process $e\pi^\pm \rightarrow e\gamma\pi^\pm$.

From table 1-3, we can see that, one by one, diagrams in the second line of fig.2 does not equal to those of the first line. From the numerical results of later sections, we will be able to see that, as a total, the second line diagrams also does not equal to those of the first line. So in this problem, the number of independent diagrams is 10 instead of 5. Of course, the total number is 20 as we indicate in the caption of fig.2.

4 Analytical Results of Electron VCS and Qualitative Properties of Pion VCS

From the aspect of experiencing VCS, unpolarized electrons and pions are similar to each other, so we can hope cross sections of VCS on the unpolarized electrons and on pions have similar v and θ dependence. Because electron has no internal structure, its VCS cross sections can be get analytically. By the same kinematical variables as those of pion VCS, neglecting the mass of the electron, we can get the following expressions for electron VCS $\gamma_\epsilon^* e \rightarrow \gamma_{\epsilon'} e$,

$$\begin{aligned} d\sigma_{RR} &\sim \bar{v} |M_{RR}|^2 \\ &\sim \frac{1}{c^2} [v^2(c^4 + 2s^2) - v(c^4 + 4s^4 + 3) + (c^2 + 1)^2] \end{aligned} \quad (11)$$

$$\begin{aligned} d\sigma_{LR} &\sim \bar{v} |M_{LR}|^2 \\ &\sim \frac{1}{c^2} [v^2(c^4 + 2s^2) - v \cdot 2s^2 + s^4] \end{aligned} \quad (12)$$

$$\begin{aligned} d\sigma_{+R} &\sim \bar{v} |M_{+R}|^2 \\ &\sim v^2 s^2 \end{aligned} \quad (13)$$

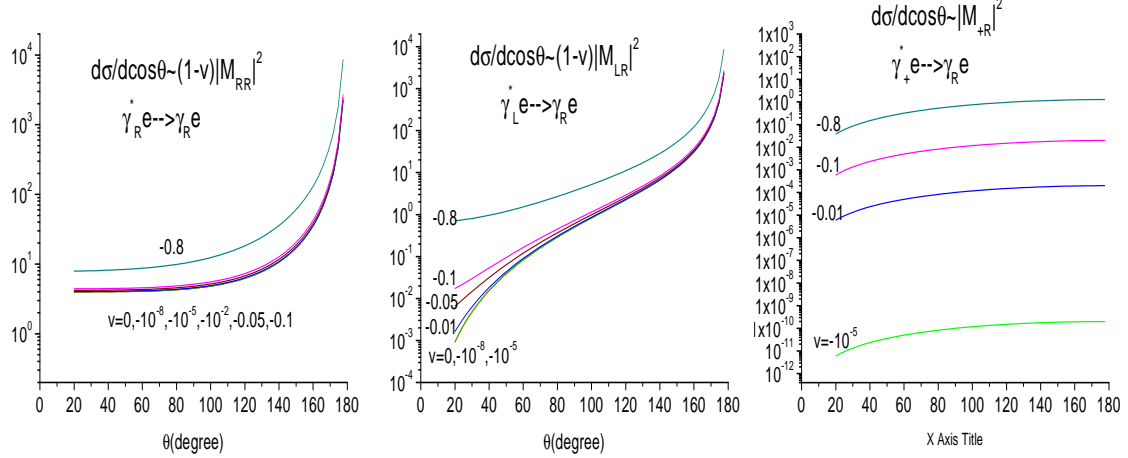


Figure 3: VCS on the unpolarized electron.

Fig.3 illustrated explicit shape of the v and θ dependence the cross sections. As we will indicate in the next section, for all the polarized cross sections $\frac{d\sigma_{eR}}{d\cos\theta}$, similarities exist between pion VCS and that of the unpolarized electron VCS.

5 Numerical Integrations and Results

We perform numerical integrations and give results for the cross sections as well as corresponding phases for different polarized processes in this section.

With eqs.(1), (2), (6) and table 1-3, and using the following relation[5]

$$S^3 \frac{d\sigma_{\epsilon\epsilon'}(\theta)}{d\cos\theta} = \frac{1}{2} \bar{v} S^4 \frac{d\sigma_{\epsilon\epsilon'}(\theta)}{dt} = \bar{v} \frac{S^2}{32\pi} |M_{\epsilon\epsilon'}|^2, \quad (14)$$

and the principle integration formula,

$$\begin{aligned} \int dx dy \frac{f(x, y)}{x - a(y) + i\epsilon} &= P \frac{f(x, y)}{(x - a)} - i\pi \int_0^1 dx dy f(x, y) \delta(x - a), \\ P \frac{f(x, y)}{x - a} &= P \frac{f(x, y) - f(a, y)}{x - a} + f(a, y) \log \frac{1 - a}{a}, \end{aligned} \quad (15)$$

we can get reliable numerical results for the cross sections and corresponding phases for different polarization processes. One can see that our treatment of the singular point appearing in the numerical integration is the subtraction method. As was indicated by [5] in the similar calculation for proton Compton scattering, different numerical treatments of the singular points can give consistent results as long as it is applied appropriately.

We get our numerical integrations by VEGAS program [16]. As did by [3], we take $\alpha_s = 0.3$, $\alpha_e = 1/136.036$ in numerical computations. Noting the fact that, H , thus M varies with $\frac{1}{S}$, we show the product $\frac{S^3 d\sigma_{ee'}(\theta)}{d\cos\theta}$ instead of $\frac{d\sigma_{ee'}(\theta)}{d\cos\theta}$ in final results.

First, in fig.4, we tried our best in reconstructing the results of [3] for the cross section $S^3 \frac{d\sigma_{+R}}{d\cos\theta}$ of pion VCS using distribution amplitudes ϕ_{p3} . From this figure, we can see that, except one point, $S^3 \frac{d\sigma_{+R}}{d\cos\theta} \not\rightarrow 0$. This is different from the case of electron VCS and from the results of [3]. It must be notified that this is not the results of our numerical methods, it is the results of the nontrivial structure of the pion. In fact, from table 3, we can get

$$H_{+R}|_{v \rightarrow 0} = \frac{16}{9} \frac{cs^{-1}[(\bar{y} - y) - 2s^2(x - y)]}{\bar{x}y[x(1 - ys^2) - c^2y + i\epsilon]} \quad (16)$$

Obviously, eq.(16) is not antisymmetrical on exchanging x, y or y, \bar{y} , so it cannot be zero after integration with the symmetry factor $\phi(x, \bar{x})\phi(y, \bar{y})$. The non-zero terms come from the diagrams d, e, i, j of fig.2, with photons attached to different quarks. There is no such corresponding diagrams in the electron case.

In fig.5, we illustrated the v dependence of the cross sections and corresponding phases for different polarized processes, with distribution amplitude ϕ_{as} . For $\gamma_+^* \pi \rightarrow \gamma_R \pi$ process, the cross section decreases with $v \rightarrow 0$, but except one point, it is nonzero when $v = 0$. For $\gamma_L^* \pi \rightarrow \gamma_R \pi$ and $\gamma_R^* \pi \rightarrow \gamma_R \pi$ process, the cross sections decrease as $v \rightarrow -1$ at large scattering angles. In the little angle region, the trend reverses. When $v \rightarrow 0$, the phase of $M_{LR} \rightarrow 180^\circ$, if we redefine the domain of the phase angle, it can be set to 0. It should be notified that, when $v = 0, \theta = 90^\circ$, the cross section $S^3 d\sigma_{+R}/d\cos\theta = 0$ exactly, so a deep well and a jump change take place in fig.5. This is different from the nearly jumping appearing in fig.5 of [3].

In fig.6, we compared distribution amplitudes from different models and their effects on the physical observables. From this figure, we can see that, relative to ϕ_{as} and ϕ_{cz} , the end-point-region suppressed distribution amplitudes ϕ_{bhl} and ϕ_{hs} [15] do not give suppressed cross sections for the scattering process. This is natural because when ϕ_{bhl} (ϕ_{hs}) suppresses the endpoint region, it intensifies the center region greatly. This point can also explain the fact that the center and end point region both intensified distribution amplitude ϕ_{p3} always gives the largest cross sections in all cases.

From the calculation of diagrams in fig.2, we know that the momentum transferred through the gluon propagator depends on x and y strongly. For example, in fig.2(a), the momentum transferred through the gluon propagator is $(\bar{x}k - \bar{y}k')^2 =$

$2\bar{x}\bar{y}k \cdot k'$. So, if the end point region of the distribution amplitudes has very important contributions to the cross sections of the physical process, pQCD is non-applicable in this problem. Now, our results indicate that the very end point region, $x \rightarrow 0, 1$ region, does not have so strong contributions to physical predictions. So our calculation is self consistent, at least in the case of pion Compton scattering.

To see this more clearly, we computed another six polarized cross sections for virtual Compton scattering process in fig.7. The upper part of fig.7 corresponds to the $v = -0.05$ case while the down part corresponds to the $v = -0.8$ case. As in fig.6, we can see that the end-point-region suppressed distribution amplitudes do not give suppressed cross sections for the physical processes. However, the center and end point region both intensified distribution amplitude ϕ_{p3} always gives largest cross sections for physical processes.

Comparing the results of pion VCS figs.5, 6 and those of electron case fig.3, we can easily see that the two kinds of processes are similar to each other, for the scattering angle dependence as well as v dependence of the cross sections. This may serve as a support for the reliability of our numerical computations.

6 Conclusions

We recalculated pion VCS in pQCD in this paper, RCS is treated as a limit case in our framework. Comparisons with existing literatures and with electron VCS are made in the text. Our study of different distribution amplitudes and their effects on the cross sections and corresponding phases of the polarized processes indicates that pQCD calculations for pion VCS are self consistent.

Acknowledgements

The first author thanks very much to Professor Hsiang-nan Li for his suggestion of studying an exclusive process as the beginning of pQCD learning. He is also very grateful to the anonymous referee for the kind instructions and suggestions. This work is partially supported by the National Natural Science Foundation of China.

References

- [1] SELEX Collaboration, hep-ex/0109003.
- [2] M. Tamazouzt, Phys. Lett. B 211 (1988) 477.
- [3] E. Maina, R. Torasso, Phys. Lett. B 320 (1994) 337.
- [4] G.R. Farrar, H. Zhang, Phys. Rev. D 41 (1990) 3348.
- [5] T. Brooks, L. Dixon, Phys. Rev. D 62 (2000) 114021.
- [6] A. S. Kronfeld, B. Nizic, Phys. Rev. D44 (1992) 3445, D46 (1992) 2272(E).
- [7] C. Coriano, H-n. Li, Nucl. Phys. B434 (1995) 535.
- [8] G. P. Lepage, S. J. Brodsky, Phys. Rev. D 22 (1980) 2157.
- [9] J. Botts, G. Sterman, Nucl. Phys. B325 (1989) 62;
H-n. Li, G. Sterman, Nucl. Phys. B381 (1992) 129.
- [10] M. A. Shifman, A. I. Vainshtein, V. I. Zakharov, Nucl. Phys. B147 (1979) 385
- [11] V. L. Chernyak, A. R. Zhitnitsky, Phys. Rept. 112 (1984) 173 and reference there in.
V. L. Chernyak, A. R. Zhitnitsky, Nucl. Phys. B201 (1982) 492.
- [12] S. V. Mikhailov, A. V. Radyushkin, Phys. Rev. D. 45 (1992) 1754;
A. V. Radyushkin, CEBAF-TH-94-13;
V. M. Braun, I. E. Filyalov, Z. Phys. C 44 (1989) 157.
- [13] G. R. Farrar, K. Huleihel, H. Zhang, Nucl. Phys. B349 (1991) 655.
- [14] T. Huang, B.-Q. Ma, Q.-X. Shen, Phys. Rev. D49 (1994) 1490.
- [15] T. Huang, Q.-X. Shen, Z. Phys. C 50 (1991) 139.
- [16] G.P. Lepage, J. Comput. Phys. 27 (1978) 192.
- [17] R.D. Field, Applications of perturbative QCD, Addison Wesley Publishing Company, Redwood City, USA, 1989.
- [18] M.T. Grisaru, H.N. Pendleton and P. van Nieuwenhuizen, Phys. Rev. D 15 (1977) 996;
M.T. Grisaru and H.N. Pendleton, Nucl. Phys. B124 (1977) 81;
S.J. Parke and T.R. Taylor, Phys. Lett. B 157 (1985) 81, err. ibid. B 174 (1986) 465;
M.L. Mangano and S.J. Parke, Phys. Rept. 200 (1991) 301.

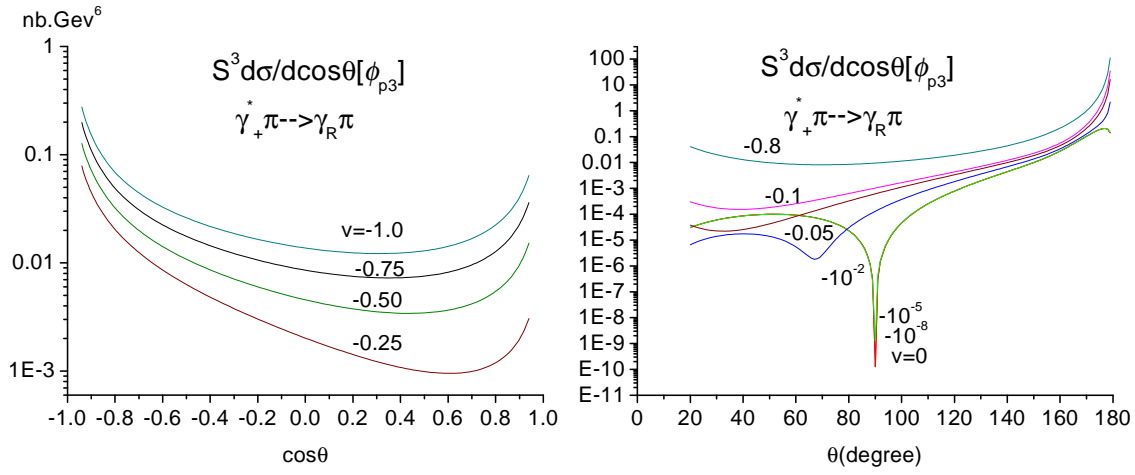


Figure 4: Left part, results reconstructed for $S^3 \frac{d\sigma_{+R}}{d\cos\theta}$ of [3]. Except a total factor, our results coincide with [3]. Right part, unlike the conclusion of [3], we found that when $v \rightarrow 0$, $S^3 \frac{d\sigma_{+R}}{d\cos\theta} \not\rightarrow 0$, except at the point $\theta = 90^\circ$.

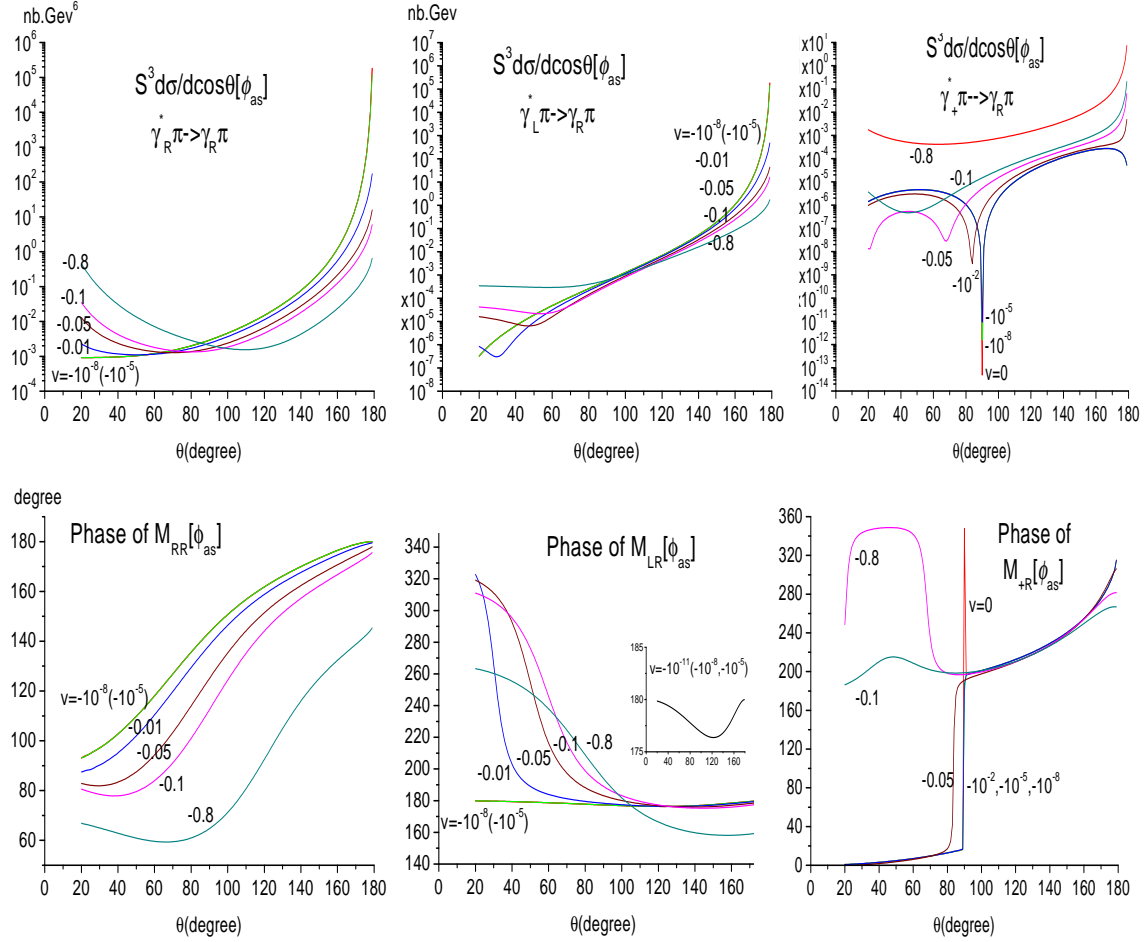


Figure 5: Effects of input photons virtuality on the polarized cross section and corresponding phases. The distribution amplitude involved is ϕ_{as} . As $v \rightarrow 0$, the phase of $M_{LR} \rightarrow 180$ asymptotically. The jumping change appearing in the phase of M_{+R} happens at the position $v = 0, \theta = 90^\circ$, where the corresponding cross section equals to zero exactly, so it is reasonable.

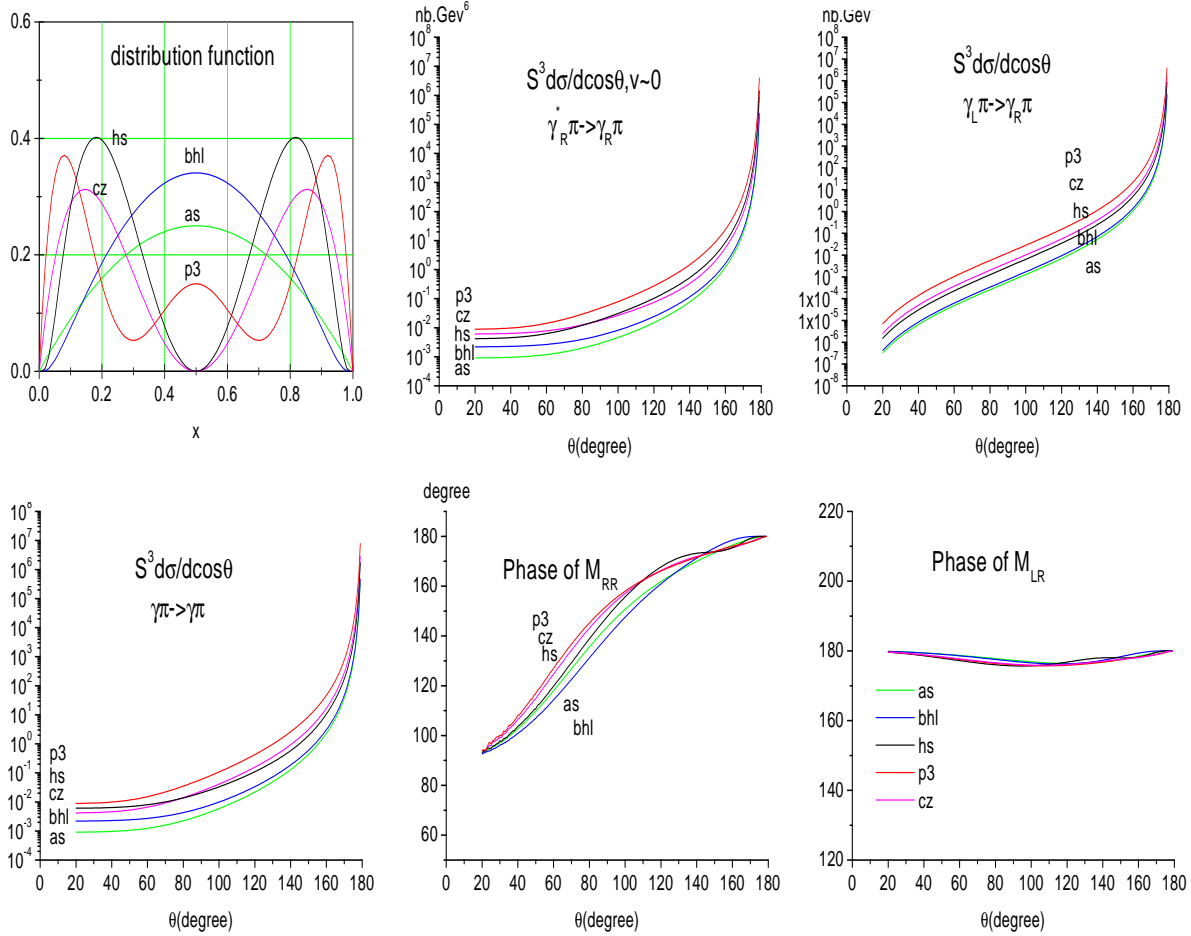


Figure 6: Distribution amplitudes and their effects on the real Compton scattering process. Because in operations, we take $v = -10^{-10}$ as real Compton scattering limit, the phase of M_{LR} does not equal to 180° precisely. Relative to ϕ_{as} and ϕ_{cz} , functions ϕ_{bhl} and ϕ_{hs} suppress the end point region deeply, but the corresponding cross sections suffer little suppression.

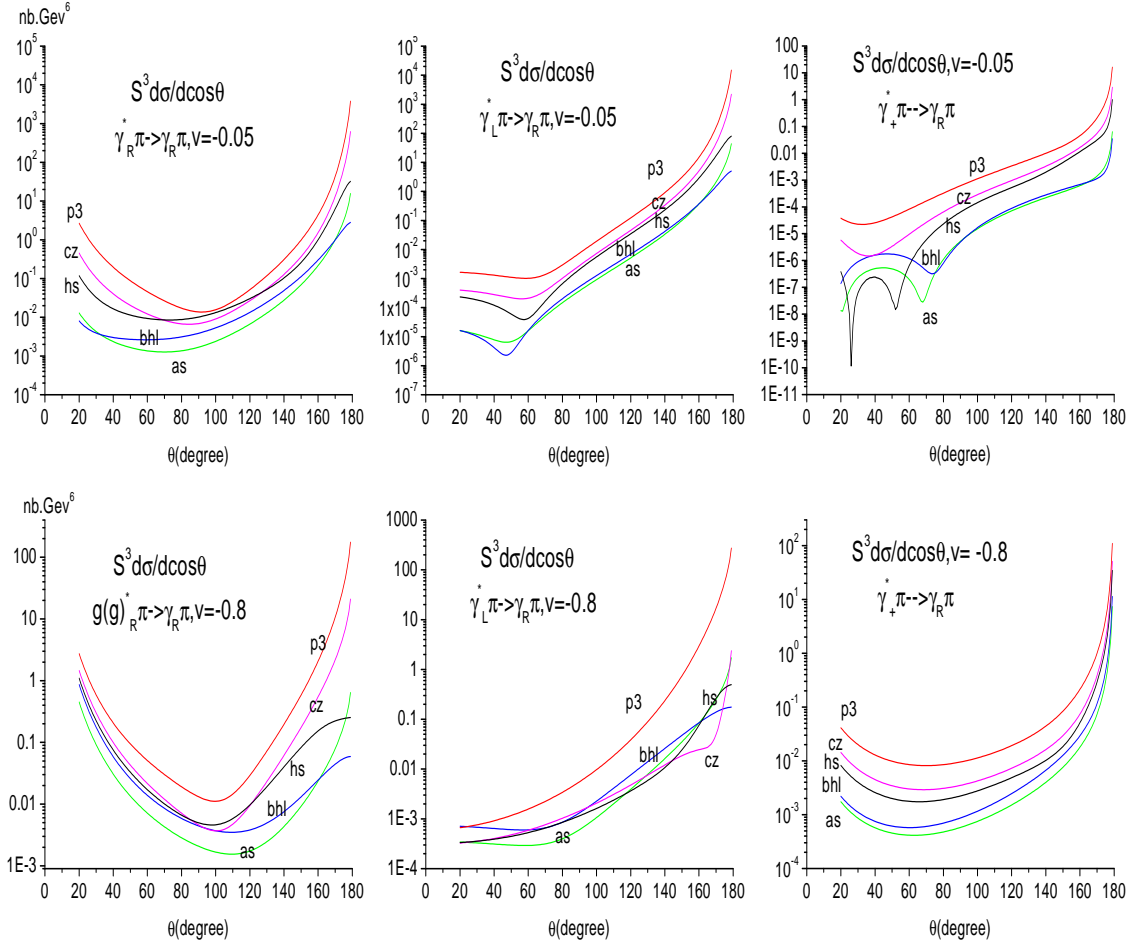


Figure 7: Further study of effects from distribution amplitudes on the cross sections of polarized virtual Compton scattering. The center and end point region both intensified distribution amplitude ϕ_{p3} always gives the largest cross sections.

